



# Up-Converting Lanthanide-Doped YAG Nanospheres

Marta Vallés-Pelarda, Rafael S. Sanchez, Eva M. Barea, Iván Mora-Seró and Beatriz Julián-López\*

Institute of Advanced Materials, Universitat Jaume I, Castellón de la Plana, Spain

The development of lanthanide-doped  $Y_3Al_5O_{12}$  (Ln:YAG) garnet nanostructures is a hot topic in the field of inorganic nanophosphors due to the current interest in developing small nanoparticles for solid-state lighting (SSL), displays, lasers and scintillation applications. In this study, we report the preparation of homogeneous Ln:YAG (Ln: Ho/Yb ions) nanospheres through a combined two-steps coprecipitation-solvothermal synthesis at low temperature. The crystal growth takes place in ethylene glycol, which is an inexpensive, non-toxic and easily available solvent. Monodisperse and crystalline spherical YAG particles of 80 nm in diameter were obtained. Furthermore, the protocol can be extended to other compositions (Tb/Yb, Tm/Yb...) to explore different luminescent properties, without affecting the morphology of the material, indicating the robustness and practical utility of the reported methodology. Thermal treatment of the nanogarnets at 1200°C is necessary for making materials optically active upon both UV and NIR excitation. The spherical morphology of annealed samples is preserved, what helps their further dispersion in solvents, barbotines, inks or printing vehicles. The lanthanide-doped nanogarnets exhibited the characteristic blue, green and red emissions from lanthanide upconversion photoluminescence (UCPL) upon NIR excitation. The UCPL mechanism was studied and CIE chromate coordinates were obtained. These nanogarnets were further evaluated as functional ceramic phosphors by incorporating them into commercial glazes. The materials exhibited an exceptional chemical stability in a harsh medium such as a fused glaze. Consequently, the visible emissions of the nanoparticles were transferred to the whole glass matrix, thus providing a functional glaze that emits intense blue and green light upon NIR excitation. These luminescent nanogarnets have promising applications in smart enamels, but can also be useful for lighting displays (white LEDs...), smart paintings or plastics, and anti-counterfeiting systems.

**Keywords:** nanogarnets, up-conversion, solvothermal approach, luminescence, ceramic glazes

## INTRODUCTION

Yttrium aluminum garnets (YAG:  $Y_3Al_5O_{12}$ ) represent one of the most important photonic material as host matrix for luminescent trivalent lanthanide ions. As bulk material, YAG has excellent chemical stability, hardness, high thermal conductivity, high UV to mid-IR transparency and low-energy phonons of the garnet structure (Blasse and Brill, 1967). Therefore, lanthanide-doped YAG materials have been used for full-color phosphors and solid-state white lighting by

## OPEN ACCESS

### Edited by:

Lothar Wondraczek,  
Friedrich Schiller University Jena,  
Germany

### Reviewed by:

Xiaoyong Huang,  
Taiyuan University of Technology,  
China  
John Ballato,  
Clemson University, United States

### \*Correspondence:

Beatriz Julián-López  
julian@uji.es

### Specialty section:

This article was submitted to  
Ceramics and Glass,  
a section of the journal  
Frontiers in Materials

**Received:** 20 May 2020

**Accepted:** 22 July 2020

**Published:** 07 August 2020

### Citation:

Vallés-Pelarda M, Sanchez RS,  
Barea EM, Mora-Seró I and  
Julián-López B (2020) Up-Converting  
Lanthanide-Doped YAG  
Nanospheres. *Front. Mater.* 7:273.  
doi: 10.3389/fmats.2020.00273

changing the doping materials, such as Ce, Tb, Eu, and Tm (Kang et al., 2000; Hsu et al., 2003; Zhou et al., 2003; Zhang et al., 2009; Ye et al., 2010; Xia and Meijerink, 2017).

However, by reducing the particle size, new potentialities arises. For instance, ultra-fine grains can be used for high-resolution display devices (Kolesov et al., 2011; Zhang et al., 2014). The use of nanoparticles in LED lighting can reduce photon scattering and improve its overall performance (Haranath et al., 2006; Venkatramu et al., 2010). In addition, nano-sized YAGs are of interest to prepare transparent ceramics for lasers and scintillators (Ma et al., 2018).

The synthesis of YAG is usually performed through solid-state reactions at high temperature (above 1300°C). However, the low reaction rate of the diffusion processes implies very long reaction times and the material usually exhibits chemical heterogeneities and high crystal size 5–20 μm (Malinowski et al., 1999; Chenais et al., 2003). The advance on bottom-up synthetic approaches allowed to obtain crystalline garnets at much lower temperature with a good control on morphology at the nanoscale (Birkel et al., 2012; Pavasaryte et al., 2015; Armetta et al., 2019). Therefore, garnet nanostructures are very promising materials for technological applications as laser materials (doped with Nd<sup>3+</sup>, Yb<sup>3+</sup>, Er<sup>3+</sup>) (Ikesue and Aung, 2008), for white lighting (doped with Ce<sup>3+</sup>) (Wei et al., 2012; Ma et al., 2015) or for hydrogen storage applications (Salehabadi et al., 2018).

Some works reported on the solvothermal synthesis of YAG-based materials with interesting nanostructures (Li et al., 2004a,b; Zhang et al., 2004). In these reports, sub 100 nm-sized YAG and Ce-doped YAG phosphors with spherical shape were prepared envisaging applications in various types of display panels. This interesting methodology led to crystalline nanoparticles at around 300°C, what supposes a dramatic reduction of the reaction temperature, as compared to solid-state reactions, and represents great energy savings. However, to our knowledge, this approach has not been extended to other lanthanide-doped YAG materials, which could offer tailor-made luminescence properties.

Furthermore, in last years, garnets with multimodal luminescence have appeared as attractive materials for new display devices and for enhancing the conversion efficiency of next generation solar cells via spectral modification (Mishra et al., 2014) or radiation detectors (Odziornek et al., 2018). Indeed, nanogarnets exhibiting upconversion (UC) photoluminescence (PL) (Wang and Liu, 2009; Haase and Schäfer, 2011) have gained interest for quantum information storage and processing (Kolesov et al., 2012), or biomedical applications, such as nanoheating and nanothermometry in the first biological window (Marciniak et al., 2017; Lozano-Gorrin et al., 2018). However, the studied systems are basically gallium-based garnets with infrared-to-visible light conversion (Pandozzi et al., 2005; Venkatramu et al., 2012; Rathaiah et al., 2015).

The interest in upconverting yttrium aluminum nanoparticles is increasing (Diaz-Torres et al., 2005; Li et al., 2005; Liu et al., 2007; Jain et al., 2018; Kamińska et al., 2020) because these materials can find applications in a wide variety of fields such as biomedicine, encoding, sensors, energy, security, and so on (Van der Ende et al., 2009; Chen and Xiaojun Zhao, 2012; Chen

et al., 2014; Wang et al., 2015; Zhou et al., 2015; Kłonkowski et al., 2018). In this context, there is plenty of room for new materials based on lanthanide-doped YAG nanogarnets with upconversion properties.

This work presents the synthesis of Ln:YAG (Ln: Ho/Yb, Tb/Yb and Tm/Yb pairs) nanogarnets in a two-steps route: precipitation and solvothermal treatment at 220°C. The synthesis takes place in ethylene glycol, which is an inexpensive, non-toxic and easily available solvent. The study of the crystalline structure and morphology, as well as the Stokes and upconversion luminescence properties for the different compositions is detailed.

Finally, the stability and functionality of these upconverting YAG nanomaterials in ceramic glazes is assessed. This work demonstrates the possibility to use these nanooxides as UC additives, instead of the most used fluoride systems (i.e., NaYF<sub>4</sub>:Ln), for applications requiring high temperature or harsh environments, in which fluorides are not stable.

## MATERIALS AND METHODS

### Chemicals

Yttrium nitrate hexahydrate [Y(NO<sub>3</sub>)<sub>3</sub>·6H<sub>2</sub>O, 99.9%, Alfa Aesar], aluminum nitrate non-hydrate [Al(NO<sub>3</sub>)<sub>3</sub>·9H<sub>2</sub>O, 98%, Panreac, 99.997%, Aldrich], terbium nitrate [Tb(NO<sub>3</sub>)<sub>3</sub>·5H<sub>2</sub>O, 99.9%, Aldrich], ytterbium nitrate [Yb(NO<sub>3</sub>)<sub>3</sub>·5H<sub>2</sub>O, 99.9%, Strem Chemicals], thulium nitrate hexahydrate [Tm(NO<sub>3</sub>)<sub>3</sub>·6H<sub>2</sub>O, 99.9%, Strem Chemicals], holmium nitrate pentahydrate [Ho(NO<sub>3</sub>)<sub>3</sub>·5H<sub>2</sub>O, 99.9%, Aldrich], ethanol (synthesis grade, Scharlau), ammonia (Scharlau, 32%) and ethylene glycol (J.T. Baker, 99%) were used as received for the synthesis of the materials.

### Synthesis of Lanthanide-Doped Garnet Nanospheres

Nanogarnets with different compositions were obtained through a simple two-step synthetic procedure based on a coprecipitation reaction of metallic salts in basic medium, followed by a solvothermal treatment in ethylene glycol. The solvothermal treatment was performed in order to induce crystallization as well as to control the morphological features of the nanocrystals.

The stoichiometry of the synthesized phosphors was Y<sub>3</sub>Al<sub>5</sub>O<sub>12</sub> and Y<sub>2.67</sub>Ln<sub>0.03</sub>Yb<sub>0.3</sub>Al<sub>5</sub>O<sub>12</sub> (with Ln<sup>3+</sup> = Ho<sup>3+</sup>, Tb<sup>3+</sup> or Tm<sup>3+</sup>) for the host matrix and the lanthanide-doped garnets, respectively. The selection of the composition (Y<sub>3-x-y</sub>Ln<sub>x</sub>Yb<sub>y</sub>Al<sub>5</sub>O<sub>12</sub> with x = 0.03 and y = 0.3) is based on studies on YAG structures reported in the literature for which efficient upconversion responses were obtained (Liu et al., 2007; Mishra et al., 2014; Kamińska et al., 2020). The samples are respectively referenced as YAG, HoYAG, TbYAG, and TmYAG.

As a general procedure, the synthesis starts by dissolving stoichiometric amounts of the metal salts to prepare 1 g of the selected nanogarnet into 50 mL of distilled water. Then, diluted ammonia (16.5 mL of NH<sub>3</sub> in 36.5 mL of distilled water) was dropwise added to the previous solution under vigorous stirring. The final pH of the mixture was adjusted to 9.50 (checked by an

electronic pH-meter) for ensuring the complete precipitation of the metal ions as a mixture of metal hydroxides (Burriel et al., 2008). The solid was then collected by centrifugation and washed with distilled water (3 times) to remove the residual nitrates and ammonium ions. Once dried, the solid was redispersed in 70 mL of ethylene glycol and placed into a teflon-lined stainless steel autoclave (125 mL, from Paar Instruments). The system was heated at 220°C for 20 h. After that, the autoclave was cooled down to room temperature. The resulting powder was collected by centrifugation, washed with ethanol (3 times), and finally dried in air at 80°C. The as-prepared samples were further annealed at 1200°C for 2 h at a heating rate of 5°C/min in order to consolidate their crystallinity and to increase their photoluminescence properties. Thus, this work mainly address the study of calcined samples.

## Preparation of Photoluminescent Ceramic Glazes

The lanthanide-doped nanogarnets were incorporated into commercial ceramic glazes to assess their applicability. Photoluminescent ceramic glazes were prepared by mixing 25 g of the standard powdered matte frit (supplied by QuimiCer S. A., a Spanish company working on ceramic products for tiles manufacturing) with 15 mL of water in a planetary ball mill (FRITSCH pulverisette 6) for 5 min at 300 rpm. Then, a small amount of the desired nanogarnet (0.12 g) was added to 1.2 mL of the previous paste (or barbotine) and manually grinded in an agate mortar for 20 min. A coating of 0.3 mm thickness of this paste was deposited onto third-fire ceramic tiles. The glazed tiles were calcined with the appropriate firing cycle for the commercial matte glazes (shown in **Supplementary Figure S1**).

## Characterization Techniques

The X-ray diffraction (XRD) analysis was conducted using a D4 Endeavor diffractometer from Bruker-AXS, with a Bragg-Brentano ( $\theta/2\theta$ ) geometry, Cu X-ray source, diffracted axis monochromator and spark detector. The XRD patterns were measured in a  $2\theta$  range of 10°–80°, with a step of 0.05 and 1.5 s/step. The goniometer is controlled with the D4 Endeavor from Bruker AXS.

Scanning Electron Microscopy (SEM) was performed on a LEO 440i microscope equipped with an energy dispersive spectroscopy system INCA 250 (Oxford) using an acceleration voltage of 20 kV, a measurement time of 100 s, a working distance 25 nm and a calculation ratio of 1.2 k. The powdered samples were coated with Au-Pt.

High-resolution SEM micrographs were taken on a JEOL 7001F instrument (field-emission scanning electron microscope, FESEM) equipped with an energy dispersive spectroscopy (EDS) system INCA 350 (Oxford) and a wavelength dispersive system INCA Wave 200 (Oxford). The powdered samples were coated with Au-Pt. The absorption spectra were measured on a Cary 500 Scan UV-VIS-NIR spectrophotometer (Varian) equipped with an integrating sphere. The reference sample used was BaSO<sub>4</sub>. The PL spectra of the powders were recorded using two quartz microscope slides.

Photoluminescence (PL), both emission and excitation spectra, were registered on a Fluorolog from Horiba Jobin Yvon spectrophotometer. For the upconversion photoluminescence, an infrared laser diode from Roithner LaserTechnik was used as pump source. The laser diode was directly coupled to the spectrophotometer. The infrared laser diode, RLMDL-980-2W module (980 ± 5 nm, 2 W cw, stability <5%, laser head 141 × 46 × 73 nm), enables to vary the output power.

## RESULTS AND DISCUSSION

The X-ray diffraction analysis of the as-synthesized materials revealed a crystalline structure, as shown in **Figure 1** for the host matrix (YAG) and holmium-doped sample (HoYAG). The diffraction peaks (indexed in **Figure 1**) can be associated to the Y<sub>3</sub>Al<sub>5</sub>O<sub>12</sub> garnet structure (PDF card number 82-0575) as single phase. After annealing at 1200°C, a small narrowing of the diffraction peaks, indicate that crystalline domains have slightly enlarged. The XRD profiles of the pure YAG and the three doped systems synthesized in this work (Ho, Tb, and Tm) appeared very similar (**Supplementary Figure S2**).

The average crystallite size (*D*) of the samples were estimated using Scherrer's equation (Eq. 1):

$$D = \frac{K\lambda}{\beta \cos \theta} \quad (1)$$

where *K* = 0.94,  $\lambda$  represents the wavelength of K $\alpha$ Cu (1.5418 Å),  $\beta$  is the full width at half maximum of the diffraction peak

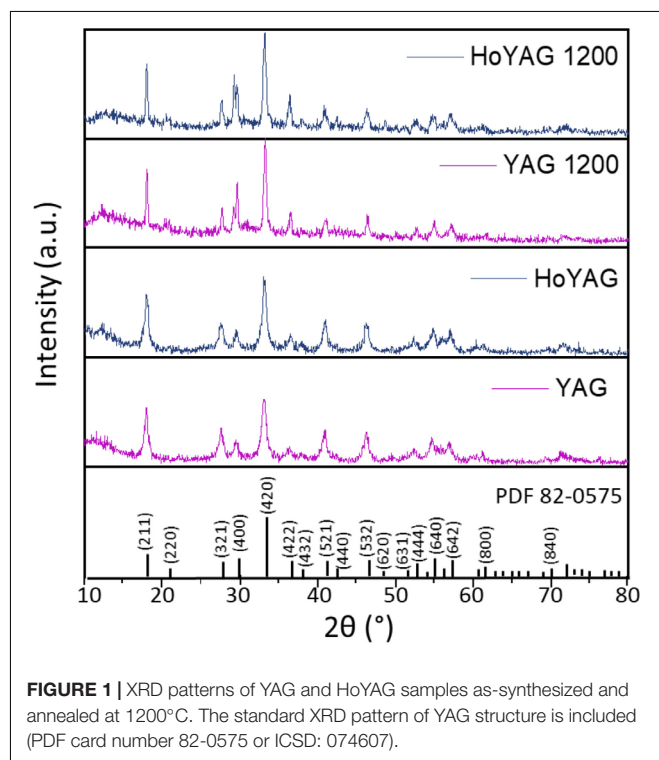


**FIGURE 1** | XRD patterns of YAG and HoYAG samples as-synthesized and annealed at 1200°C. The standard XRD pattern of YAG structure is included (PDF card number 82-0575 or ICSD: 074607).

(FWHM) and  $\theta$ (rad) is Bragg angle. The most intense diffraction peak of each sample was used for D calculation.

**Table 1** shows the average crystallite size estimated for the as-synthesized samples, which ranges from 12 to 16 nm as a function of the doping ion. After annealing process, a subtle increase of the crystallite size was observed. The most important change was detected for the matrix (YAG), from 12.4 to 23.0, meanwhile doped samples experimented a discrete or negligible crystallite size increase.

In addition, small shifts toward higher  $2\theta$  in the diffraction peak positions were detected on the doped samples as compared to YAG, but also with the annealing at 1200°C. According to Bragg's law, these shifts are associated to shorter interplanar (hkl) distances. The shift with the annealing treatment can be attributed to a contraction of the lattice because of the reduction of structural defects and a densification of the crystalline structure. The shifts in the Ln-doped garnets can be associated to the differences in ionic radii between yttrium and the lanthanide ions ( $Y^{3+}$  1.159 Å,  $Yb^{3+}$  1.125 Å,  $Tb^{3+}$  1.180 Å,  $Ho^{3+}$  1.155 Å,  $Tm^{3+}$  1.134 Å) (Shannon and Prewitt, 1969). Since 10% of  $Y^{3+}$  ions is replaced by  $Yb^{3+}$  ions (with a smaller radius), a shift of the peaks toward higher angles are expected in all the doped materials when compared to those of the YAG pattern. The second lanthanide (Ho, Tb or Tm) was incorporated in a very low amount (1% molar  $Y^{3+}$  substitution), so it is difficult to notice a clear tendency on the interplanar distances.

For a more accurate XRD analysis, structural refinements were performed with a software package MAUD (Lutterotti et al., 1997), as shown in **Supplementary Figure S3**, and the lattice parameters have been obtained (**Table 1**, see **Supplementary Table S1** for a more complete description). A decrease in the lattice parameters was observed in the as-synthesized YAG garnets doped with the lanthanide pairs (Ho/Yb, Tb/Yb and Tm/Yb) as compared to pure YAG. This result fits well with the mentioned shift of the peaks, which is explained by the smaller radii of the doping ions than yttrium in the native garnet structure, then, confirming the formation of solid solutions according to the initial stoichiometry  $Y_{2.67}Ln_{0.03}Yb_{0.3}Al_5O_{12}$  (with  $Ln^{3+} = Ho^{3+}, Tb^{3+}$  or  $Tm^{3+}$ ). With annealing, all systems exhibited a lattice contraction. This reduction can be associated to a decrease in the amount of defects and dislocations density (Guerbous and Boukerika, 2015). However, this lattice contraction is more pronounced in the non-doped sample (a

varies  $\sim 0.05$  Å for pure YAG, meanwhile 0.01–0.03 Å for the doped ones). Two possible arguments could explain this behavior. The first hypothesis would be the higher ability of the lanthanide ions to enhance nucleation during the solvothermal reaction, affording more condensed and less defective structures from the beginning. The second possibility would be that lanthanide-doped garnets have a more distorted structure than the garnet matrix and, therefore, the crystalline network is less affected by temperature. A more detailed study would be required to better explain this behavior. This would be an interesting piece of work, but is out of the scope of the present research.

Scanning Electron Microscopy images revealed that the samples were composed of aggregates of monodisperse spherical particles of  $\sim 80$  nm in diameter, as shown in **Figure 2** for HoYAG sample, even after annealing at 1200°C. Moreover, no significant differences were found in the particles shape and size of doped and undoped garnet samples (see images from **Supplementary Figure S4**), what evidences the robustness of the synthetic procedure and the efficient control of the crystal growth by ethylene glycol. In our synthesis, ethylene glycol acts as solvent but also as complexing agent at the surface of the small oxide nuclei, thus inhibiting an uncontrolled growth and shaping the nanocrystals (Dong et al., 2015a; Pavasaryte et al., 2015). We want to highlight the interesting spherical morphology, as well as the small and homogeneous size exhibited for all the compositions after annealing at 1200°C (at which the materials are optically interesting). Sub-100 nm and rounded nanocrystals are features of vital importance when nanoparticles are going to be dispersed in a liquid vehicle or medium of application (organic solvents, aqueous suspensions, inks, paintings, polymers, and so on).

The chemical composition of the materials was determined by EDS analyses. **Supplementary Figure S5** illustrates the presence of Y, Al, and O as the main chemical elements in all samples. **Supplementary Table S2** includes the semiquantitative analysis with the atomic weight of detected elements. For the undoped garnet, the atom ratio of Y/Al/O was close to the nominal composition of  $Y_3Al_5O_{12}$ . For doped garnets, Yb was clearly identified from its characteristic energy lines and the Y/Al/Yb/O atomic weights fit quite well with the stoichiometry (see **Supplementary Table S2** for detailed compositions), in which  $Yb^{3+}$  ions have substituted the  $Y^{3+}$  sites. The second doping ions, Ho, Tb or Tm, were also detected. However, their low amount (1% molar) in the samples provided values close to the detection limits of the instrument. Therefore, the analysis is not reliable for these ions, but anyway, the Ln ratio is in the order of the nominal composition.

**Figure 3** shows the UV-VIS-NIR absorption spectra of as-synthesized and annealed YAG and HoYAG samples, as illustrative examples (see **Supplementary Figure S6** for those of the other lanthanide doped systems). The spectrum of the as-synthesized undoped garnet shows an absorption band (marked with an asterisk) at 315 nm that shifts to 380 nm after annealing at 1200°C. The band gap of the host matrix is reported to be around 190 nm (Palik, 1997), a wavelength out of our possibilities of detection (also, the quartz holder absorbs below 200 nm). Therefore, the detected band at 315 nm can be associated to surface defects from the garnet structure (Rotman, 1997).

**TABLE 1** | Average crystallite size (D) and lattice parameter (a) of the synthesized garnet samples.

| Sample       | D (nm) | a (Å)  |
|--------------|--------|--------|
| YAG          | 12.4   | 12.102 |
| YAG 1200°C   | 23.0   | 12.050 |
| HoYAG        | 13.6   | 12.080 |
| HoYAG 1200°C | 18.9   | 12.071 |
| TbYAG        | 14.6   | 12.086 |
| TbYAG 1200°C | 18.9   | 12.051 |
| TmYAG        | 16.9   | 12.087 |
| TmYAG 1200°C | 17.7   | 12.073 |

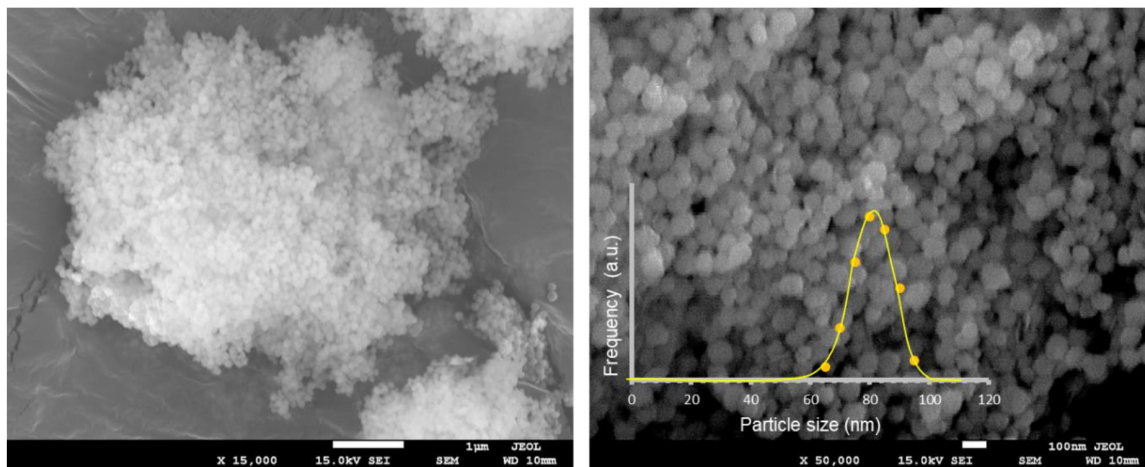


**FIGURE 2** | SEM micrographs at two different magnifications of HoYAG sample annealed at 1200°C. Inset: Particle size distribution obtained by counting particles from SEM images (250 nanoparticles).

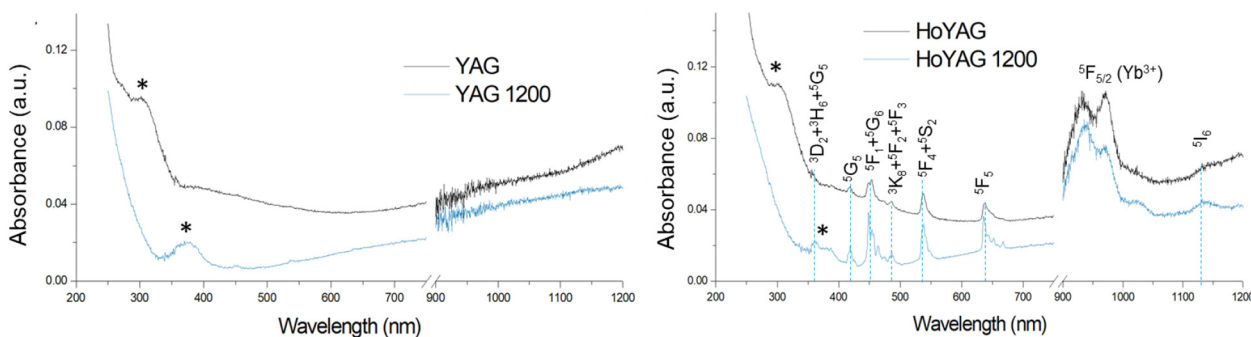


**FIGURE 3** | Absorption spectra of as-synthesized and annealed YAG and HoYAG samples. Absorptions from garnet surface defects (\*) and electronic  $4f-4f$  transitions from  $\text{Ho}^{3+}$  and  $\text{Yb}^{3+}$  ions.

With annealing, the sintering process and the crystalline growth reduce the energy of these surface defects, leading to a red-shift of the band up to 380 nm (Rotman, 1997). No more significant bands were found in the visible and near infrared range for the matrix.

The absorption spectra of Ln-doped YAG samples, besides the surface defects absorption, exhibited the bands typical from  $4f-4f$  transitions of the trivalent lanthanide ions. In the case of HoYAG, the absorptions from the ground states of the doping ions, i.e.,  $\text{Ho}^{3+}$  ( $5I_8$ ) and  $\text{Yb}^{3+}$  ( $2F_{7/2}$ ), to the different excited states were clearly detected (Malinowski et al., 2000). After annealing, the absorptions become more intense and narrower since the ions are located in more defined coordination site within the garnet structure. For TbYAG and TmYAG samples, the absorption peak of  $\text{Yb}^{3+}$  ( $2F_{7/2} \rightarrow 2F_{5/2}$  transition) at  $\sim 950\text{--}980$  nm was present. However, the low amount of  $\text{Tb}^{3+}$  and  $\text{Tm}^{3+}$  ions in the samples provided very low intense bands. Only the band from  $\text{Tm}^{3+}$  ( $3H_6 \rightarrow 3F_3$  transition) at  $\sim 680$  nm was clearly observed.

Steady-state photoluminescence (PL) of the annealed nanogarnets was performed upon UV excitation. The undoped garnet did not exhibit any emission when irradiated at

wavelengths between 250 nm (at shorter wavelengths the quartz holder absorbs) and 350 nm (limit of the visible range), indicating that the matrix is not photoluminescent, as expected. **Supplementary Figure S7** shows the PL emission spectrum of YAG upon excitation at 272 nm, as an example. **Supplementary Figure S7** also depicts the excitation spectra (in black) of the lanthanide-doped garnets recorded with the detector fixed at the most characteristic emission of the active ions ( $\text{Ho}^{3+}$ ,  $\text{Tb}^{3+}$ , or  $\text{Tm}^{3+}$ ). In the three spectra, an excitation band located at 320 or 370 nm depending on the system, was observed. This UV-blue band can be associated to the excitation of the host matrix, revealing an optical communication between matrix and the emitting ions.

Then, emission spectra were performed upon excitation at the corresponding UV-blue band, and the PL spectra are shown in red in **Supplementary Figure S7**. Most of the typical emission lines from the  $f-f$  transitions of lanthanide ions ( $\text{Ho}^{3+}$ ,  $\text{Tb}^{3+}$ , or  $\text{Tm}^{3+}$ ) can be detected. The assignment of these bands is included in the plots. The presence of the lanthanide emissions upon excitation on the matrix reveals an efficient energy transfer from the host garnet to the doping ions. The high intensity

of the emission bands observed in the spectrum of TbYAG, as compared to HoYAG or TmYAG, could be due to the fact that Tb ion has an allowed f-d transition from  $^5F_1$  level to  $5d^1$  state at around 270 nm (Chen et al., 1999; Li et al., 2005) which overlaps the garnet absorption, then increasing the energy transfers and the PL efficiency.

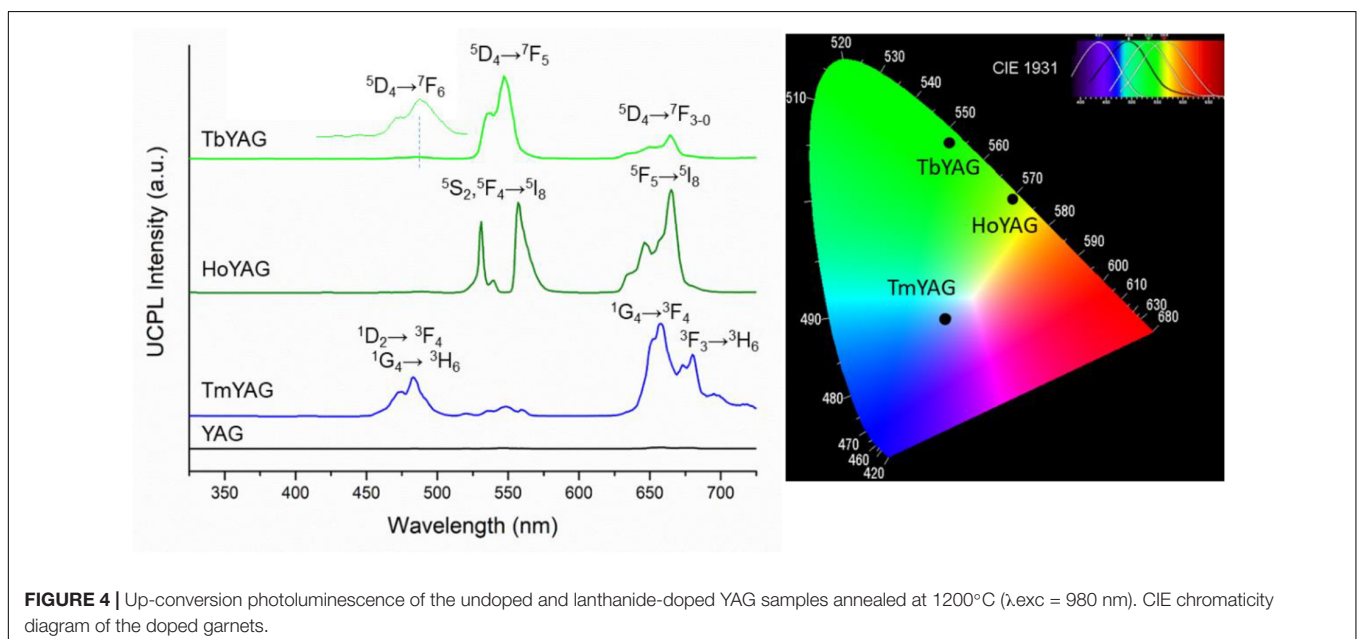
The upconversion (UC) luminescence spectra of the nanogarnets were obtained upon continuous irradiation at 980 nm (diode laser). **Figure 4** shows the UC spectra of the undoped and doped nanogarnets after annealing at 1200°C.

The as-synthesized samples did not show any photoluminescence upon NIR excitation. This behavior reveals that, although the sample exhibited a crystalline structure after the solvothermal synthesis, it is a highly defective lattice and the spatial arrangement of the  $Yb^{3+}$  and the emitting ions in the structure was not adequate to operate upconversion processes. The distribution of the active ions is especially important in the UCPL because, as a difference of the typical PL, the up-conversion phenomenon is a non-linear process that requires a subsequent two-photon absorption in which both lanthanides are implicated. Moreover, it is very dependent on the matrix phonon energy, which can absorb photons and activate non-radiative relaxations. Even, we cannot discard the presence of some residual PL quencher species (such as O-H or C-H groups) from the synthesis in the materials. Therefore, the annealing of the nanogarnets prepared in this work was necessary in order to exhibit light emission from up-conversion processes.

The expected emissions from the lanthanide ions ( $Ho^{3+}$ ,  $Tm^{3+}$ , and  $Tb^{3+}$ ) ions were observed in the visible range (Fu et al., 2014; Dong et al., 2015b). These emissions come from the excited emitting energy levels from the active ions that are populated via sensitization of the  $^2F_{5/2}$  energy level from  $Yb^{3+}$ , directly excited by the laser at 980 nm, as shown in the energy level diagrams of **Figure 5**. The UC spectrum of the TmYAG

sample exhibited the characteristic blue emissions at around 460–480 nm from  $^1D_2 \rightarrow ^3F_4$  and  $^1G_4 \rightarrow ^3H_6$  transitions and the lower energetic red emission centered at  $\sim 660$  nm from  $^1G_4 \rightarrow ^3F_4$  transition. The UC spectrum of HoYAG provides a green emission at  $\sim 530$  to  $\sim 560$  nm from  $^5S_2, ^5F_4 \rightarrow ^5I_8$  transitions and a red emission at 645 nm from  $^5F_5 \rightarrow ^5I_8$  relaxation. The UC spectrum of Tb-doped system shows characteristic peaks of the  $Tb^{3+}$  ion centered at 540 nm and 650–670 nm owing to the  $^5D_4 \rightarrow ^7F_5$  and  $^5D_4 \rightarrow ^7F_{3-0}$  electronic transitions, respectively. The pair Tb/Yb was of interest to us, since  $Tb^{3+}$  ions do not have an absorber level close in energy to the 980 nm laser excitation, but  $Yb^{3+}$  is an efficient absorber and can give a cooperative emission by the involvement of a  $Yb^{3+}-Yb^{3+}$  ion pair (Lai et al., 2008; Xue et al., 2015). This energy may be transferred to the  $^5D_4$  level of  $Tb^{3+}$ , which could open the possibility for UC emission from the  $Tb^{3+}$  ion.

CIE chromaticity diagram of the annealed nanogarnets under 980 nm excitation wavelength is presented in **Figure 4**. The color coordinates of the light emitted by the holmium and terbium doped samples are in the green region because of the contribution of  $Ho^{3+}$  and  $Tb^{3+}$  radiative relaxations at around 530–560 nm. The red emissions appearing in the UCPL spectra of these samples influence the greenish tone, as shown in the CIE diagram. Indeed, the TbYAG sample shows a deeper green hue; meanwhile the HoYAG has a more yellowish green color. The color of the light emitted by the thulium-doped system is roughly blue, even if the sample has also an important red component. The blue emission appears more intense to naked eye upon 980 nm excitation, therefore the point in the CIE diagram is located in this blue-red region. The CIE diagram coordinates are in good agreement with the light emitted by the annealed nanogarnets in powder upon excitation with laser at 980 nm when observed at naked eye, as shown in **Figure 6**.



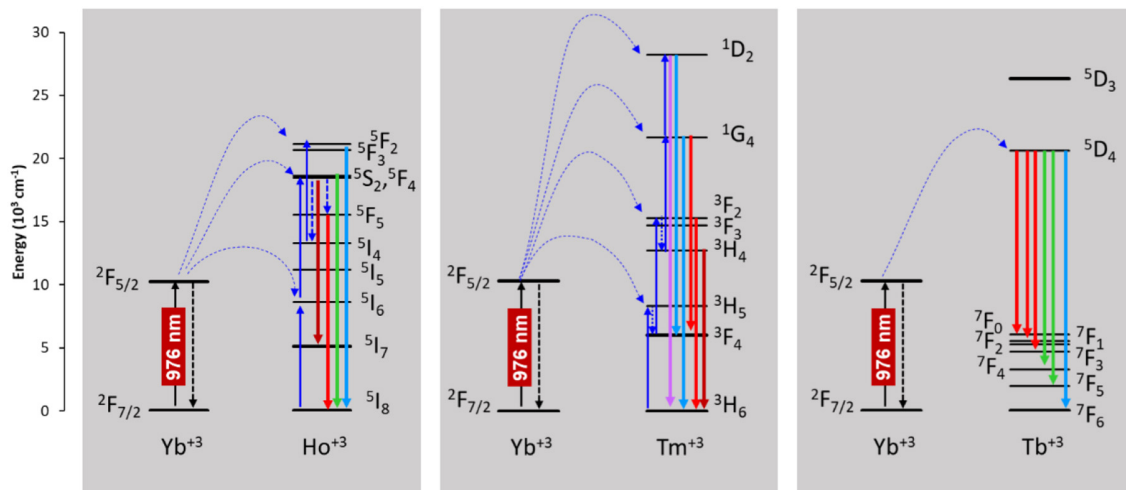


**FIGURE 5** | Energy level diagrams of the active ions responsible for the upconversion photoluminescence.

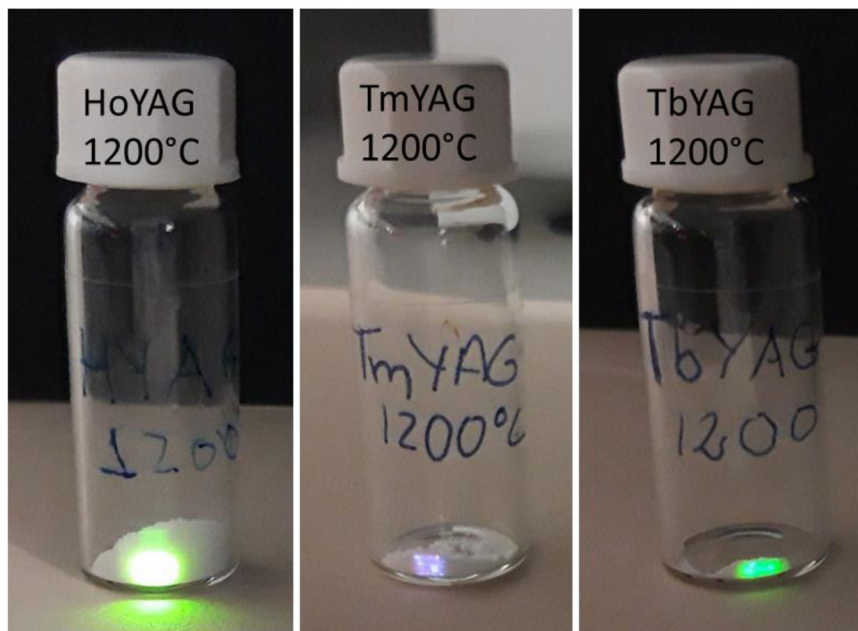


**FIGURE 6** | Pictures of the green and blue emission observed at naked eye when the annealed powders are excited upon NIR excitation (980 nm). The pictures have been taken using a hot mirror filter between the camera and the samples.

The mechanism of the UC process for the lanthanide emissions was studied in the annealed nanogarnets. The UC phenomenon follows the non-linear relationship (Eq. 2):

$$I_{UC} \propto P^n \tag{2}$$

where  $I_{UC}$  is the UC emission intensity,  $P$  is the excitation power density and  $n$  is the number of photons needed to produce the fluorescence (Pollnau et al., 2000). The intensity of the upconversion emission was calculated as the integrated area under the most intense emission of each lanthanide. The log  $I_{UC}$

vs. log  $P$  was represented. The slope of the fitting curves provided the number of photons involved in the optical up-converting mechanism. **Figure 7** represents the log-log plots for the three synthesized nanogarnets.

The dependence of the UC intensity in HoYAG, studied for the  $^5S_2 \rightarrow ^5I_8$  emission (located at 550 nm) exhibited a linear behavior with an  $n$  value of  $2.74 \pm 0.13$ . This value can be interpreted as a quadratic (two-photon) mechanism, in which several energy processes involving higher excited levels occur simultaneously, thus giving a value that does not fit with an integer. In the case of the annealed TbYAG, the  $^5D_4 \rightarrow ^7F_5$  emission (located at 540 nm)

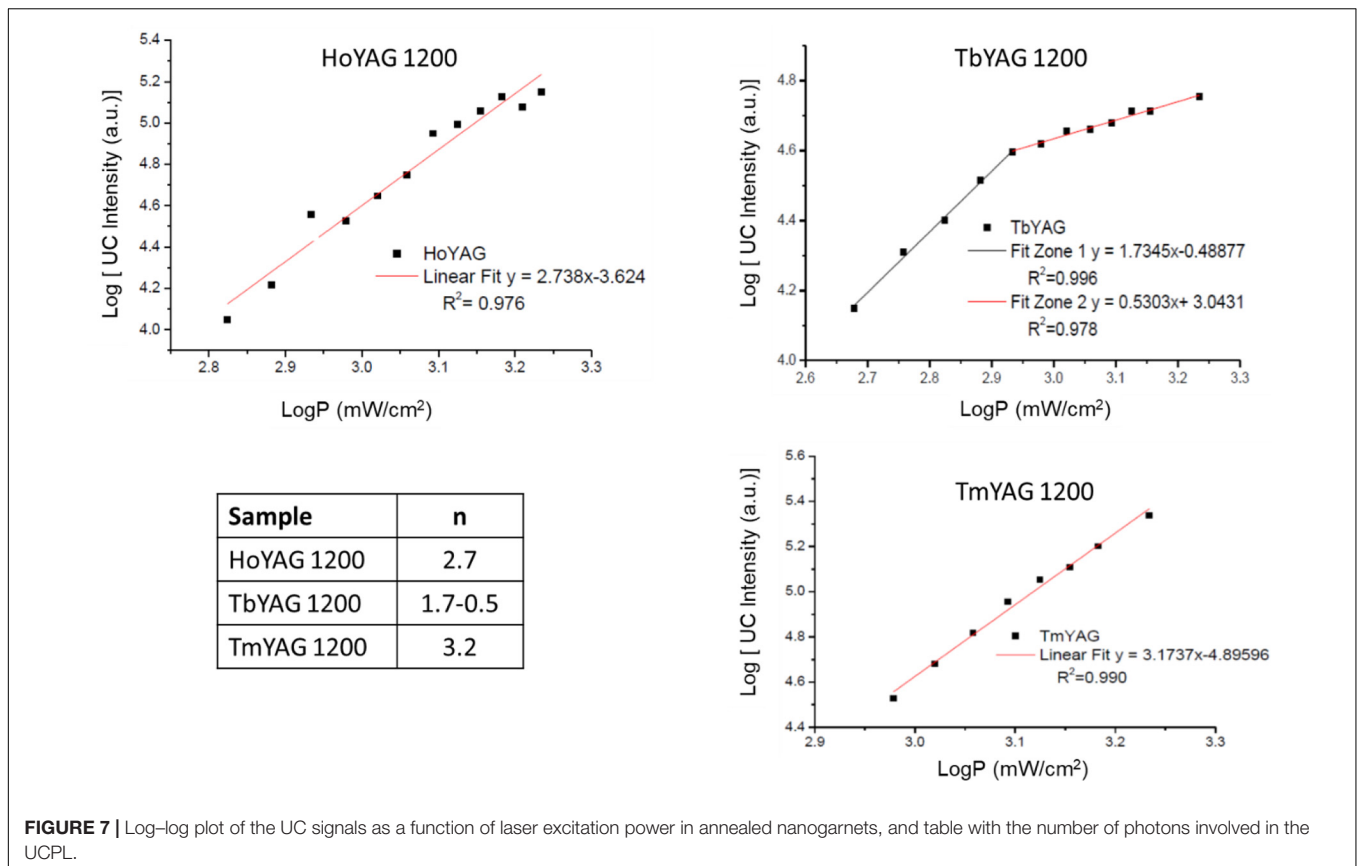


**FIGURE 7** | Log-log plot of the UC signals as a function of laser excitation power in annealed nanogarnets, and table with the number of photons involved in the UCPL.

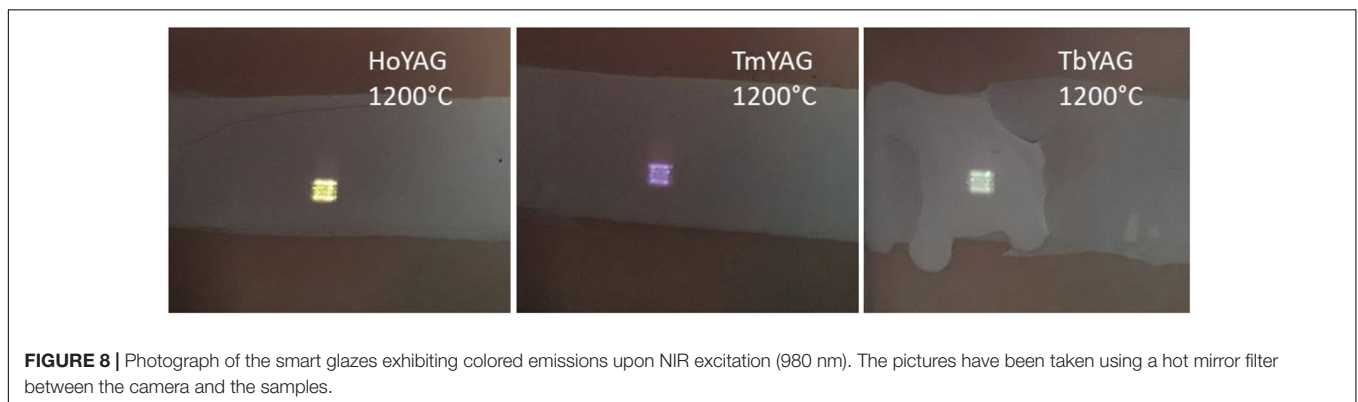


**FIGURE 8** | Photograph of the smart glazes exhibiting colored emissions upon NIR excitation (980 nm). The pictures have been taken using a hot mirror filter between the camera and the samples.

exhibited a power dependence of  $1.73 \pm 0.06$  until a power density of  $0.85 \text{ mW/cm}^2$ , indicating a two-photon mechanism. At higher power, the  $n$ -value decreases up to  $0.53 \pm 0.03$ , meaning that the UC luminescence is approaching saturation. For the third system, TmYAG, the  ${}^1\text{G}_4 \rightarrow {}^3\text{F}_4$  emission (located at 680 nm) exhibited a power dependence of  $3.17 \pm 0.12$  associated to a three-photon mechanism.

The intense colored light when irradiated at NIR (980 nm) and the interesting morphological features of these nanogarnets can find interest in different fields of applications such as sensors, biological applications, security, lighting or smart paintings and glazes.

In order to assess their applicability as additives for functional luminescent glazes, a commercial ceramic matte glaze was employed. A bright glaze would difficult the optical evaluation of the materials. For that, a small amount of the annealed garnet powders were incorporated into the glass barbotine (<5%). Then, a 3 mm coating was deposited on the surface of a ceramic tile and fired at the appropriate temperature (according to the firing cycle shown in **Supplementary Figure S1**).

The functional ceramic glazes exhibited an intense blue or green light emission when irradiated upon 980 nm, as shown in **Figure 8**, thus corroborating that the upconverting properties from the nanogarnets were completely preserved.

This result indicates that the garnet nanospheres have an exceptional chemical stability in the harsh medium of a fused glaze. Therefore, these luminescent nanogarnets can have promising applications in smart enamels, but also in optical devices such as LEDs or for anti-counterfeiting systems in different media (paintings, plastics, porcelains, etc.).

## CONCLUSION

This work has presented a robust and green synthetic route, based on a coprecipitation-solvothermal methodology at low temperature (220°C), for the preparation of monodisperse lanthanide doped YAG nanospheres. The use of ethylene glycol as the reaction medium provided garnet nanoparticles of 80 nm with different compositions, i.e., Ln:YAG (Ln: Ho/Yb, Tb/Yb, and Tm/Yb pairs). SEM analyses showed an interesting spherical morphology, which is of great interest for their dispersion in different application media (solvents, barbotines, inks, paintings or printing vehicles).

XRD patterns reflected crystalline structure in the as-synthesized samples, and lattice parameters were in good agreement with the formation of solid solutions in the doped garnets. After annealing at 1200°C, the crystallinity was enhanced and the network was slightly contracted, as expected by the sintering process and the reduction of the matrix defects.

Absorption spectra revealed the presence of matrix defects in the UV-blue region, together with the characteristic absorption from the ground states to  $4f$  energy levels of the lanthanide ions, in the visible (for Ho, Tb, and Tm) and NIR (Yb) regions.

The Stokes photoluminescence of the nanogarnets presented the typical emission bands from the lanthanide ions upon UV excitation. More interestingly, intense blue, green and red emissions from Tm, Ho, and Tb ions were detected in the annealed samples upon NIR excitation at 980 nm. The as-synthesized sample did not exhibit emission under similar conditions, probably due to the presence of lattice defects, residual quenchers such as OH or CH groups, or to an unsuitable spatial arrangement of the optically-active ions in the as-synthesized garnet lattice unable to operate upconversion processes. After annealing, the intense colored emissions were attributed to the activation of  $f-f$  transitions via  $\text{Yb}^{3+}$  sensitization. The UCPL mechanisms were studied and CIE chromatic coordinates were found in good agreement with the color of the samples at naked eyes.

The nanogarnets were evaluated as additives in commercial glazes to get functional ceramic phosphors. The modified commercial glazes emitted intense blue or green light upon NIR radiation, corroborating that nanogarnets are stable in that

medium. Furthermore, the luminescence of the nanogarnets have been transferred to the whole glass coating. Thus, we believe that these luminescent and highly stable nanogarnets can find new applications in smart ceramic materials, and be of interest for new generation of lighting displays (white LEDs...), functional paintings and plastics, and security and anti-counterfeiting applications.

## DATA AVAILABILITY STATEMENT

All datasets generated for this study are included in the article/**Supplementary Material**, further inquiries can be directed to the corresponding author.

## AUTHOR CONTRIBUTIONS

MV-P: materials synthesis, investigation, and draft preparation. RS: support on optical characterization. EB: support on synthesis and characterization. IM-S: supervision and resource. BJ-L: resource, supervision, data curation, and manuscript writing. All authors have read and agreed to the published version of the manuscript.

## FUNDING

This research has been supported by the European Research Council (ERC) via Consolidator Grant (724424-No-Limit Project), Generalitat Valenciana (Prometeo, 2018/098), and Universitat Jaume I (Nenuphar project UJI-B2018-71 and DEPE2D project UJI-B2019-09). MV-P acknowledges Universitat Jaume I for her Ph.D. Fellowship Program (PREDOC/2017/40).

## ACKNOWLEDGMENTS

Serveis Centrals d'Instrumentació Científica from Universitat Jaume I is acknowledged for instrumental facilities. Fabrizio Guzzetta is acknowledged for his help on XRD refinements.

## SUPPLEMENTARY MATERIAL

The Supplementary Material for this article can be found online at: <https://www.frontiersin.org/articles/10.3389/fmats.2020.00273/full#supplementary-material>

## REFERENCES

Armetta, F., Saladino, M. L., Giordano, C., Defilippi, C., Marciniak, L., Hreniak, D., et al. (2019). Non-conventional Ce:YAG nanostructures via urea complexes. *Sci. Rep.* 9:3368. doi: 10.1038/s41598-019-39069-6

Birkel, A., Denault, K. A., George, N. C., Doll, C. E., Héry, B., Mikhailovsky, A. A., et al. (2012). Rapid microwave preparation of highly efficient  $\text{Ce}^{3+}$ -substituted garnet phosphors for solid state white lighting. *Chem. Mater.* 24, 1198–1204. doi: 10.1021/cm300238

Blasse, G., and Bril, A. (1967). Activated phosphors. *J. Chem. Phys.* 47, 5139–5145.

- Burriel, F., Lucena, F., Arribas, S., and Hernández, J. (2008). *Química Analítica Cualitativa*. Madrid: Editorial Paraninfo.
- Chen, G. Y., Qju, H. L., Prasad, P. N., and Chen, X. Y. (2014). Upconversion nanoparticles: design, nanotechnology, and applications in theranostics. *Chem. Rev.* 114, 5161–5214. doi: 10.1021/cr400425h
- Chen, J., and Xiaojun Zhao, J. (2012). Upconversion nanomaterials: synthesis, mechanism, and applications in sensing. *Sensors* 12, 2414–2435. doi: 10.3390/s120302414
- Chen, T.-M., Chen, S. C., and Yu, C. J. (1999). Preparation and characterization of garnet phosphor nanoparticles derived from oxalate coprecipitation. *J. Sol. State Chem.* 144, 437–441. doi: 10.1006/jssc.1999.8202
- Chenais, S., Druon, F., Balembois, F., Georges, P., Brenier, A., and Boulon, G. (2003). Diode-pumped Yb:GGG laser: comparison with Yb:YAG. *Opt. Mater.* 22, 99–106. doi: 10.1016/S0925-3467(02)00353-1
- Diaz-Torres, L. A., De la Rosa, E., Salas, P., and Desirena, H. (2005). Enhanced cooperative absorption and upconversion in Yb<sup>3+</sup> doped YAG nanophosphors. *Opt. Mater.* 27, 1305–1310. doi: 10.1016/j.optmat.2004.10.020
- Dong, H., Chena, Y.-C., and Feldmann, C. (2015a). Polyol synthesis of nanoparticles: status and options regarding metals, oxides, chalcogenides, and non-metal elements. *Green Chem.* 17, 4107–4132. doi: 10.1039/C5GC00943J
- Dong, H., Sun, L. D., and Yan, C. H. (2015b). Energy transfer in lanthanide upconversion studies for extended optical applications. *Chem. Soc. Rev.* 44, 1608–1634. doi: 10.1039/C4CS00188E
- Fu, L., Xia, H., Dong, Y., Li, S., Gu, W., Zhang, J., et al. (2014). Upconversion luminescence from terbium and ytterbium codoped LiYF<sub>4</sub> single crystals. *J. Alloys Comp.* 617, 584–587. doi: 10.1016/j.jallcom.2014.08.053
- Guerbous, L., and Boukerika, A. (2015). Nanomaterial host bands effect on the photoluminescence properties of Ce-Doped YAG nanophosphor synthesized by Sol-Gel method. *J. Nanomat.* 2015:617130. doi: 10.1155/2015/617130
- Haase, M., and Schäfer, H. (2011). Upconverting nanoparticles. *Angew. Chem. Int. Ed.* 50, 5808–5829. doi: 10.1002/anie.201005159
- Haranath, D., Chander, H., Sharma, P., and Singh, S. (2006). Enhanced luminescence of Y<sub>3</sub>Al<sub>5</sub>O<sub>12</sub>:Ce<sup>3+</sup> nanophosphor for white light-emitting diodes. *Appl. Phys. Lett.* 89:173118. doi: 10.1063/1.2367657
- Hsu, W. T., Wu, W. H., and Lu, C. H. (2003). Synthesis and luminescent properties of nano-sized Y<sub>3</sub>Al<sub>5</sub>O<sub>12</sub>:Eu<sup>3+</sup> phosphors. *Mater. Sci. Eng. B* 104, 40–44. doi: 10.1016/S0921-5107(03)00268-X
- Ikesue, A., and Aung, Y. L. (2008). Ceramics laser materials. *Nat. Photon.* 2, 721–727. doi: 10.1038/nphoton.2008.243
- Jain, A., Gonzalez, C. A. E., Tejada, E. M., Duran, A., Contreras, O. E., and Hirata, G. A. (2018). Covering the optical spectrum through different rare-earth ion-doping of YAG nanospheres produced by rapid microwave synthesis. *Ceram. Int.* 44, 1886–1893. doi: 10.1016/j.ceramint.2017.10.127
- Kamińska, I., Jankowski, D., Sikora, B., Kowalik, P., Minikayev, R., Wojciechowski, T., et al. (2020). Structural, optical and magnetic properties of Y<sub>3</sub>-0.02-xEr<sub>0.02</sub>Yb<sub>x</sub>Al<sub>5</sub>O<sub>12</sub> (0 < x < 0.20) nanocrystals: effect of Yb content. *Nanotechnology* 31, 225711. doi: 10.1088/1361-6528/ab73b9
- Kang, Y. C., Lenggoro, I. W., Park, S. B., and Okuyama, K. (2000). YAG:Ce phosphor particles prepared by ultrasonic spray pyrolysis. *Mater. Res. Bull.* 35, 789–798. doi: 10.1016/S0025-5408(00)00257-9
- Klonkowski, A. M., Kukiński, B., Kubus, M., Ryl, J., Szczodrowski, K., Wileńska, D., et al. (2018). Up-conversion white emission and other luminescence properties of a YAG:Yb<sub>2</sub>O<sub>3</sub>:Tm<sub>2</sub>O<sub>3</sub>:Ho<sub>2</sub>O<sub>3</sub>@SiO<sub>2</sub> glass-nanocomposite. *RSC Adv.* 8, 11006–11013. doi: 10.1039/C8RA00118A
- Kolesov, R., Reuter, R., Xia, K. W., Stohr, R., Zappe, A., and Wrachtrup, J. (2011). Super-resolution upconversion microscopy of praseodymium-doped yttrium aluminum garnet nanoparticles. *Phys. Rev. B*, 8:153413. doi: 10.1103/PhysRevB.84.153413
- Kolesov, R., Xia, K., Reuter, R., Stohr, R., Zappe, A., Meijer, J., et al. (2012). Optical detection of a single rare-earth ion in a crystal. *Nat. Commun.* 3:1029. doi: 10.1038/ncomms2034
- Lai, H., Bao, A., Yang, Y., Tao, Y., Yang, H., Zhang, Y., et al. (2008). UV luminescence property of YPO<sub>4</sub>:RE (RE = Ce<sup>3+</sup>, Tb<sup>3+</sup>). *J. Phys. Chem. C* 112, 282–286. doi: 10.1021/jp074103g
- Li, X., Liu, H., Wang, J., Cui, H., Yang, S., and Boughton, I. R. (2005). Solvothermal synthesis and luminescent properties of YAG:Tb nano-sized phosphors. *J. Phys. Chem. Solids* 66, 201–205. doi: 10.1016/j.jpcs.2004.09.012
- Li, X., Liu, H., Wang, J. Y., Cui, H. M., and Han, F. (2004a). Production of nanosized YAG powders with spherical morphology and nonaggregation via a solvothermal method. *J. Am. Ceram. Soc.* 87, 2288–2290. doi: 10.1111/j.1151-2916.2004.tb07507.x
- Li, X., Liu, H., Wang, J. Y., Cui, H. M., and Han, F. (2004b). YAG:Ce nano-sized phosphor particles prepared by a solvothermal method. *Mater. Res. Bull.* 39, 1923–1930. doi: 10.1016/j.materresbull.2004.05.013
- Liu, M., Wang, S. W., Zhang, J., An, L. Q., and Chen, L. D. (2007). Upconversion luminescence of Y<sub>3</sub>Al<sub>5</sub>O<sub>12</sub> (YAG):Yb<sup>3+</sup>, Tm<sup>3+</sup> nanocrystals. *Opt. Mater.* 30, 370–374. doi: 10.1016/j.optmat.2006.11.060
- Lozano-Gorriñ, A. D., Rodríguez-Mendoza, U. R., Venkatramu, V., Monteseuro, V., Hernandez-Rodríguez, M. A., Martín, I. R., et al. (2018). Lanthanide-doped Y<sub>3</sub>Ga<sub>5</sub>O<sub>12</sub> garnets for nanoheating and nanothermometry in the first biological window. *Opt. Mater.* 84, 46–51. doi: 10.1016/j.optmat.2018.06.043
- Lutterotti, L., Matthies, S., Wenk, H.-R., Schultz, A. S., and Richardson, J. W. Jr. (1997). Combined texture and structure analysis of deformed limestone from time-of-flight neutron diffraction spectra. *J. Appl. Phys.* 81, 594–600. doi: 10.1063/1.364220
- Ma, B., Lu, T., Zhang, W., Wei, N., Lu, Z., Chen, X., et al. (2015). Microstructural sintering evolution and sintering parameters optimization of the silica-doped Nd:YAG ceramics using the co-precipitated raw powder. *J. Eur. Ceram. Soc.* 35, 2403–2412. doi: 10.1016/j.jeurceramsoc.2015.02.003
- Ma, X., Li, X., Li, J., Genevois, C., Ma, B., Etienne, A., et al. (2018). Pressureless glass crystallization of transparent yttrium aluminum garnet-based nanoceramics. *Nat. Commun.* 9:1175. doi: 10.1038/s41467-018-03467-7
- Malinowski, M., Frukacz, Z., Szufinska, M., Wnuk, A., and Kaczkan, M. (2000). Optical transitions of Ho<sup>3+</sup> in YAG. *J. Alloys Comp.* 30, 389–394. doi: 10.1016/S0925-8388(99)00770-7
- Malinowski, M., Piramidowicz, R., Frukacz, Z., Chadeyron, G., Mahiou, R., and Joubert, M. F. (1999). Spectroscopy and upconversion processes in YAlO<sub>3</sub>:Ho<sup>3+</sup> crystals. *Opt. Mater.* 12, 409–423. doi: 10.1016/S0925-3467(98)00081-0
- Marciniak, L., Bednarkiewicz, A., Drabik, J., Trejgis, K., and Strek, W. (2017). Optimization of highly sensitive YAG:Cr<sup>3+</sup>, Nd<sup>3+</sup> nanocrystal-based luminescent thermometer operating in an optical window of biological tissues. *Phys. Chem. Chem. Phys.* 19, 7343–7351. doi: 10.1039/c6cp07213e
- Mishra, K., Singh, S. K., Singh, A. K., Rai, M., Gupta, B. K., and Rai, S. B. (2014). New perspective in garnet phosphor: low temperature synthesis, nanostructures, and observation of multimodal luminescence. *Inorg. Chem.* 53, 9561–9569. doi: 10.1021/ic500854k
- Odziornek, M., Chaput, F., Dujardin, C., Lerouge, F., Cassette, P., Sitarz, M., et al. (2018). Design and application of high optical quality YAG:Ce nanocrystal-loaded silica aerogels. *ACS Appl. Mater. Interfaces* 10, 32304–32312. doi: 10.1021/acsami.8b09229
- Palik, E. D. (1997). *Handbook of Optical Constants of Solids, Five-Volume Set: Handbook of Thermo-Optic Coefficients of Optical Materials with Applications*. Cambridge, MA: Academic Press.
- Pandozzi, F., Vetrone, F., Boyer, J. C., Naccache, R., Capobianco, J. A., Speghini, A., et al. (2005). A spectroscopic analysis of blue and ultraviolet upconverted emissions from Gd<sub>3</sub>Ga<sub>5</sub>O<sub>12</sub>:Tm<sup>3+</sup>, Yb<sup>3+</sup> nanocrystals. *J. Phys. Chem. B* 109, 17400–17405. doi: 10.1021/jp052192w
- Pavasaryte, L., Julián-López, B., and Kareiva, A. (2015). Solvothermal synthesis of Eu<sup>3+</sup>-doped holmium aluminum garnet. *Mendelev Commun.* 25, 384–385. doi: 10.1016/j.mcom.2015.09.024
- Pollnau, M., Gamelin, D. R., Luthi, S. R., Gudel, H. U., and Hehlen, M. P. (2000). Power dependence of upconversion luminescence in lanthanide and transition-metal-ion systems. *Phys. Rev. B* 61, 3337–3346. doi: 10.1103/PhysRevB.61.3337
- Rathiah, M., Haritha, P., Linganna, K., Monteseuro, V., Martín, I. R., Lozano-Gorriñ, A. D., et al. (2015). Infrared-to-visible light conversion in Er<sup>3+</sup>-Yb<sup>3+</sup>:Lu<sub>3</sub>Ga<sub>5</sub>O<sub>12</sub> nanogarnets. *ChemPhysChem* 16, 3928–3936. doi: 10.1002/cphc.201500694
- Rotman, S. R. (1997). “The effect of defects on inorganic luminescent materials,” in *Wide-Gap Luminescent Materials: Theory and Applications. Electronic Materials: Science and Technology*, Vol. 2, ed. S. R. Rotman (Boston, MA: Springer), 139–190. doi: 10.1007/978-1-4615-4100-4\_3
- Salehabadi, A., Sarrami, F., Salavati-Niasari, M., Gholami, T., Spagnoli, D., and Karton, A. (2018). Dy<sub>3</sub>Al<sub>2</sub>(AlO<sub>4</sub>)<sub>3</sub> ceramic nanogarnets: Sol-gel auto-combustion synthesis, characterization and joint experimental and

- computational structural analysis for electrochemical hydrogen storage performances. *J. Alloys Comp.* 744, 574–582. doi: 10.1016/j.jallcom.2018.02.117
- Shannon, R. D., and Prewitt, C. T. (1969). Effective ionic radii in oxides and fluorides. *Acta Cryst. B* 25, 925–945.
- Van der Ende, B. M., Aarts, L., and Meijerink, A. (2009). Lanthanide ions as spectral converters for solar cells. *Phys. Chem. Chem. Phys.* 11, 11081–11095. doi: 10.1039/b913877c
- Venkatramu, V., Giarola, M., Mariotto, G., Enzo, S., Polizzi, S., Jayasankar, C. K., et al. (2010). Nanocrystalline lanthanide-doped Lu<sub>3</sub>Ga<sub>5</sub>O<sub>12</sub> garnets: interesting materials for light-emitting devices. *Nanotechnology* 21:175703. doi: 10.1088/0957-4484/21/17/175703
- Venkatramu, V., Leon-Luis, S. F., Rodriguez-Mendoza, U. R., Monteselegro, V., Manjon, F. J., Lozano-Gorrin, A. D., et al. (2012). Synthesis, structure and luminescence of Er<sup>3+</sup>-doped Y<sub>3</sub>Ga<sub>5</sub>O<sub>12</sub> nano-garnets. *J. Mater. Chem.* 22, 13788–13799. doi: 10.1039/c2jm31386c
- Wang, F., and Liu, X. (2009). Recent advances in the chemistry of lanthanide-doped upconversion nanocrystals. *Chem. Soc. Rev.* 38, 976–989. doi: 10.1039/B809132N
- Wang, M., Zhu, Y., and Mao, C. B. (2015). Synthesis of NIR-responsive NaYF<sub>4</sub>:Yb,Er upconversion fluorescent nanoparticles using an optimized solvothermal method and their applications in enhanced development of latent fingerprints on various smooth substrates. *Langmuir* 31, 7084–7090. doi: 10.1021/acs.langmuir.5b01151
- Wei, N., Lu, T., Li, F., Zhang, W., Ma, B., Lu, Z., et al. (2012). Transparent Ce:Y<sub>3</sub>Al<sub>5</sub>O<sub>12</sub> ceramic phosphors for white light-emitting diodes. *Appl. Phys. Lett* 101:4. doi: 10.1063/1.4742896
- Xia, Z. G., and Meijerink, A. (2017). Ce<sup>3+</sup>-Doped garnet phosphors: composition modification, luminescence properties and applications. *Chem. Soc. Rev.* 46, 275–299. doi: 10.1039/c6cs00551a
- Xue, X., Cheng, T., Suzuki, T., and Ohishi, Y. (2015). Upconversion emissions from high energy levels of Tb<sup>3+</sup> under near-infrared laser excitation at 976 nm. *Opt. Mater. Express* 5, 2768–2776. doi: 10.1364/OME.5.002768
- Ye, S., Xiao, F., Pan, Y. X., Ma, Y. Y., and Zhang, Q. Y. (2010). Phosphors in phosphor-converted white light-emitting diodes recent advances in materials, techniques and properties. *Mat. Sci. Eng. R Rep.* 71, 1–34. doi: 10.1016/j.mser.2010.07.001
- Zhang, R., Lin, H., Yu, Y., Chen, D., Xu, J., and Wang, Y. (2014). A new-generation color converter for high-power white LED: transparent Ce<sup>3+</sup>:YAG phosphor-in-glass. *Laser Photon. Rev.* 8, 158–164. doi: 10.1002/lpor.201300140
- Zhang, S. S., Wang, Q. P., Zhang, X. Y., Cong, Z. H., Fan, S. Z., Liu, Z. J., et al. (2009). Continuous-wave ceramic Nd:YAG laser at 1123 nm. *J. Laser Phys. Lett.* 6, 864–867. doi: 10.1002/lapl.200910094
- Zhang, X. D., Liu, H., He, W., Wang, H. Y., Li, X., and Boughton, R. I. (2004). Synthesis of monodisperse and spherical YAG nanopowder by a mixed solvothermal method. *J. Alloys Comp.* 372, 300–303. doi: 10.1016/S0925-8388(03)01133-2
- Zhou, J., Liu, Q., Feng, W., Sun, Y., and Li, F. Y. (2015). Upconversion luminescent materials: advances and applications. *Chem. Rev.* 115, 395–465. doi: 10.1021/cr400478f
- Zhou, Y. H., Lin, J., Yu, M., Han, S. M., Wang, S. B., and Zhang, H. J. (2003). Morphology control and luminescence properties of YAG:Eu phosphors prepared by spray pyrolysis. *Mater. Res. Bull.* 38, 1289–1299. doi: 10.1016/S0025-5408(03)00141-7

**Conflict of Interest:** The authors declare that the research was conducted in the absence of any commercial or financial relationships that could be construed as a potential conflict of interest.

Copyright © 2020 Vallés-Pelarda, Sanchez, Barea, Mora-Seró and Julián-López. This is an open-access article distributed under the terms of the Creative Commons Attribution License (CC BY). The use, distribution or reproduction in other forums is permitted, provided the original author(s) and the copyright owner(s) are credited and that the original publication in this journal is cited, in accordance with accepted academic practice. No use, distribution or reproduction is permitted which does not comply with these terms.